JOURNAL OF MATERIALS SCIENCE **40** (2005) 1429–1443

Organic solar cell optimizations

S. SUN*, Z. FAN, Y. WANG, J. HALIBURTON
Center for Organic Photonic Materials Research and Chemistry Department, Norfolk State University, 700 Park Avenue, Norfolk, VA 23504, USA
E-mail: ssun@nsu.edu

This paper presents recent experimental and theoretical approaches for optimizing organic solar cell efficiencies in both space and energy/time domains. Specifically, in spatial domain, a 'tertiary' block copolymer supra-molecular nano structure has been designed, and a series of −DBAB- type of block copolymers, where D is a conjugated donor block, A is a conjugated acceptor block, and B is a non-conjugated and flexible bridge unit, have been synthesized and preliminarily examined for target photovoltaic functions. For instance, in comparison to simple donor/acceptor (*D*/*A*) blend film, a corresponding −DBAB- block copolymer film exhibited much better photoluminescence (PL) quenching (from less then 70% to over 90%), biased conductivity (2–3 orders of magnitude better), and photo conductivity (100% increase). These are attributed mainly to spatial domain improvement for charge carrier generation and transportation. In energy level domain, the photo induced charge separation appears most efficient when the donor/acceptor frontier orbital energy offset is close to the sum of two major energy costs: the charge separation reorganization energy and the exciton binding energy. Other donor/acceptor frontier orbital energy offsets are also identified where the charge recombination becomes most severe, and where the charge separation rate constant over charge recombination rate constant become largest. These energy offset values are very critical for designing high efficiency organic solar cells.

1. Introduction

Sun light is a clean and renewable energy source conveniently available on the earth and in outer space. Though certain inorganic semi conductor based photovoltaic materials/devices can convert about 30% solar energy into electric power [1], organic or polymer based solar panels or sheets are very attractive for low cost, light weight, large area, and flexible shaped solar panel needs [1–14]. In addition to solar energy conversions, photovoltaic materials and devices also can be used in photo-detector applications such as in photoelectric signal transductions in optical communication or optical imaging systems. The key difference in these different applications is that, in photo-detector applications, the optical excitation energy gap (optical gap) of the photovoltaic materials must match the energy of the optical signal (e.g., 1.5 micron or 0.8 eV IR light signal in optical communications). In the case of solar cells, the materials optical excitation gap should match the solar spectrum with maximum photon flux between 1.3–2.0 eV on the surface of the earth (air mass 1.5), or 1.8–3.0 eV in outer space (air mass 0) [1–4]. Semiconducting and conducting conjugated polymers developed in recent years posses some inherent advantages, including lightweight, flexible shape, ultra-fast (up to femtosecond) opto-electronic response, nearly continuous tunability of materials energy levels and band-gaps via molecular design and synthesis, versatile materials processing and device fabrication schemes, and low cost on large scale industrial manufacturing [15]. Additionally, as research in organic photovoltaic materials are rapidly growing, key bottleneck factors, such as the 'photon losses', the 'exciton losses', and the 'carrier losses' that hinder organic/polymeric photovoltaic performance gradually become clear [14], high efficiency organic photovoltaic systems appear feasible, as all these "losses" can be minimized by systematic optimizations at space, energy and/or time domains. In this article, some fundamental mechanisms and current problems of organic photovoltaic materials and devices are briefly outlined first, then spatial domain optimizations using a 'tertiary' nano structured −DBAB- type block copolymer, and energy/time domain optimizations by identifying optimal donor/acceptor energy levels and offsets are described.

2. Fundamentals and current problems of organic photovoltaics

In order to develop high efficiency organic or polymeric photovoltaic materials and devices, a brief comparison of the classic inorganic solar cells (such as first inorganic 'Fritts Cell' [16]) versus the organic solar cells (such as first organic 'Tang Cell' [6]) would be

* Author to whom all correspondence should be addressed.

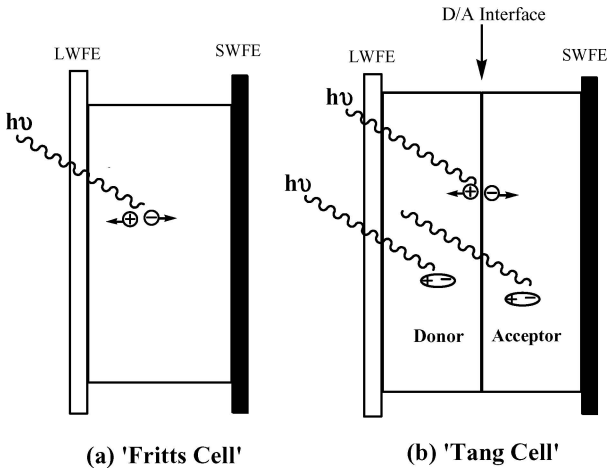

Figure 1 A schematic comparison of a classic: (a) inorganic and (b) organic photovoltaic cell.

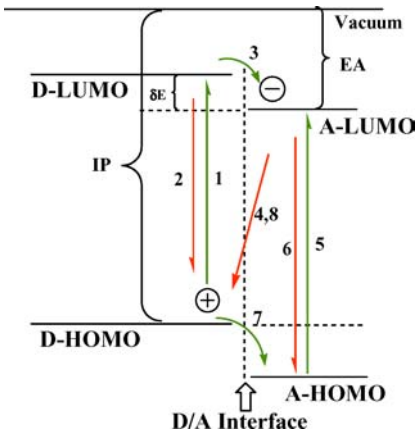

Figure 2 Scheme of frontier orbitals and photo induced charge separation and recombination processes in an organic donor/acceptor binary light harvesting system.

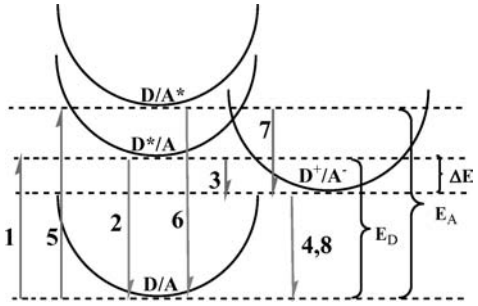

Figure 3 Scheme of standard Gibbs free-energy potential wells of photo induced charge separation and recombination processes in an organic donor/acceptor light harvesting system.

helpful. The first inorganic solar cell was reported by Charles Fritts in 1885 [16]. As illustrated in Fig. 1a, the 'Fritts' cell was composed of a semiconducting Selenium thin layer sandwiched between two different metal layer electrodes. One very thin and semi-transparent gold layer acting as a large work function electrode (LWFE) to collect photo generated positive charges (holes), and the other iron layer acting as a small work function electrode (SWFE) to collect photo generated negative charges (electrons). In 'Fritz' cell, when an energy matched photon strikes the selenium, a large (up to 10 nm) and loosely correlated 'free' electron/hole pair was generated. The electron/hole can be separated easily by room temperature thermal energy (kT, less then 0.05 eV), where the free electron would be in a conduction band (CB), and the free hole is left in the valence band (VB). The free electrons and holes (also called 'charged carriers' or simply 'carriers') can then diffuse to the respective and opposite electrodes driven by a field created by the two different work function metal electrodes.

In contrast, in the first organic solar cell ('Tang Cell') as shown in Fig. 1b, when an energy matched photon strikes an organic unit (mainly low excitation gaped π electron unit), it only generates a relatively small (1 nm or less) strongly bound and neutral electron-hole pair, called 'exciton'. It would require a much higher then room temperature energy (e.g., 0.05–1.5 eV) [17–19], also called exciton binding energy, to separate the electron from the hole. Such a neutral exciton can diffuse (e.g., via energy transfer) randomly to any direction within exciton lifetime of typically pico to nano seconds, and the average exciton diffusion length (AEDL) for organic conjugated materials is typically 10–70 nm [17–19]. Clearly, exciton itself would not generate any photovoltaic property. However, as shown in Figs 1b and 2–3, if two different organic materials with different frontier electronic orbitals are present and in direct contact to each other (via either space, or aliphatic bonds), one material has a smaller ionization potential (IP) called donor, and the other material has a larger electron affinity (EA) called acceptor (Figs 2 and 3), when a photo generated exciton (in either donor or acceptor) diffuses to the donor/acceptor interface, if the exciton is at donor side, the electron at the donor LUMO will quickly transfer into the acceptor LUMO (transfer #3 in Figs 2 and 3) driven by the LUMO level offset between the donor and the acceptor. If the exciton is at acceptor side, the hole at acceptor HOMO will jump quickly into the donor HOMO (corresponding to an electron back transfer #7 in Figs 2 and 3) driven by the HOMO level offset between the donor and the acceptor, thus an exciton now becomes a free electron (at acceptor LUMO) and a free hole (at donor HOMO) resulting in positive and negative charge separation. Now the freed electrons and holes (charged carriers) can diffuse separately to their respective electrodes, desirably in two separate donor and acceptor phases, so the chance of electron-hole recombination would be minimal. Thus, a donor/acceptor binary system appears very critical for organic photovoltaic function [6].

For an organic solar cell, the overall power conversion efficiencies are limited by at least following five steps:

(1) Photon absorption and exciton generation;
(2) Exciton diffusion to donor/acceptor interface;
(3) Exciton split or charged carrier generation at donor/acceptor interface;
(4) Carrier diffusion to respective electrodes;
(5) Carrier collection by the electrodes.

For all currently reported organic or polymeric photovoltaic materials and devices, none of the above

mentioned five steps have been optimized, it is therefore not surprising that the power conversion efficiencies of all currently reported organic or polymeric solar cells are relatively low in comparison to their inorganic counterparts.

2.1. Photon absorption and exciton generation

In this first step of organic photovoltaic, a basic requirement is that the materials optical excitation energy gap (optical gap) should be equal or close to the incident photon energy. In most amorphous organic materials where electronic band structures are difficult to form, this gap is the energy gap between the Highest Occupied Molecular Orbital (HOMO) and the Lowest Unoccupied Molecular Orbital (LUMO), both are also called frontier orbitals. In organic conjugated system, HOMO is typically an occupied π bonding orbital, and LUMO is typically an unoccupied π^* anti-bonding orbital. Since an organic LUMO/HOMO excitation basically generates a tightly bound exciton instead of a free electron and hole, "optical energy gap" is therefore used instead of the conventional "electronic energy gap" that typically refers to the energy gap between the free holes at valence band (VB) and the free electrons at conduction band (CB) in inorganic semiconducting materials [1]. In organics, the relationship of "optical gap (E_{go})" versus "electronic gap (E_{ge})" may be approximated as $E_{ge} = E_{go} + E_B$, where E_B is called exciton binding energy that represents a minimum energy needed to separate an intra-molecular exciton into an inter-molecular radical ion pair [17]. E_{go} values can be estimated directly from optical absorption band edge, and absolute E_{ge} values may be estimated by electrochemical Redox analysis. Absolute HOMO/LUMO levels are typically estimated from a referenced 'half' electrochemical analysis in combination with the optical absorption spectroscopy. For a widely used conjugated semiconducting polymer poly-*p*-phenylenevinylenes or 'PPV', for instance, the exciton binding energy has been reported to be varies between 0.05–1.1 eV [17]. For solar cell applications, solar light radiation span a wide range yet with largest photo-flux between 600–1000 nm (1.3–2.0 eV, on surface of the earth or 1.5 air mass) or 400–700 nm (1.8–3.0 eV, in space or air mass 0) [1–4]. For terrestrial applications, it is desirable that the energy gaps of a solar cell span a range from 1.3 to 2.0 eV. This may be achieved by incorporating a series of different energy gaped donor/acceptor or organic dyes that absorb light in that radiation range. However, while the solar photon loss can be minimized in this way, due to energy transfer processes where all high energy excitons will eventually become lowest energy excitons [19], the open circuit voltage (V_{oc}) of the cell will also be reduced accordingly. Experimental studies have revealed certain correlations of V_{oc} versus the gap of lowest acceptor LUMO and highest donor HOMO levels [20]. In reality, several widely used conjugated semiconducting polymers used in organic solar cell studies have optical gaps higher then 2.0 eV [15]. For instance, widely used alkyloxy derivatized poly-*p*-phenylenevinylenes (PPV) has a typical optical gap of about 2.3–2.6 eV, well above the maximum solar photon flux range at the surface of the earth. This is why the photon absorption (or exciton generation) for PPV based solar cells are far from being optimized at AM 1.5. This 'photon loss' problem is in fact very common in almost all currently reported organic photovoltaic materials and devices. However, one advantage of organic materials is the versatility and flexibility of its energy levels being fine tuned via molecular design and synthesis, therefore, ample room exists for improvement. A number of recent studies on the developments of low band gap conjugated polymers are such examples [21–23].

2.2. Exciton diffusion

Once an organic exciton is photo generated, it typically diffuses (e.g., via intra-chain or inter-chain energy transfer processes) to a remote site, and at the same time decay radiatively or non-radiatively to its ground state at typically pico to nano seconds lifetime [18, 19]. Alternatively, in solid state, some excitons may be trapped in certain defect/impurity sites. Both exciton decay and trap contribute to the "exciton loss". The average distance an organic exciton can travel within its lifetime is called average exciton diffusion length (AEDL). The AEDL depends heavily on the spatial property (morphology) of the materials. For most conjugated organic materials, the AEDL is typically in the range of 10–70 nm [1–3, 18–19]. For instance, the AEDL for PPV is around 10 nm [18]. Since the desired first step of photovoltaic process is that, each photo generated exciton is able to reach the donor/acceptor interface to incur charge separation. This means, one way to minimize the "exciton loss" would be to make a defect free material with a donor/acceptor phase separated tertiary nano structuresuch that, an exciton generated at any site of the material can reach a donor/acceptor interface in its diffusion path within the AEDL [14]. Such a structure may also be called a 'bulk hetero-junction' structure [7–8]. One limitation in the 'Tang Cell' is that, if the donor or acceptor layer is thicker then the AEDL, the 'exciton loss' would be a serious problem. On the other hand, if the photovoltaic active layer thickness is too thin, then "photon loss' due to poor light absorption would become a problem. This is also why 'bulk hetero-junction' type solar cells are desirable, as they not only minimize the exciton loss by increasing the donor/acceptor interface, they can also offer enough thickness for effective photon harvesting.

2.3. Exciton separation and charge carrier generation

Once an exciton diffuses to a donor/acceptor interface, or an exciton is photo generated nearby or at the donor/acceptor interface, the interface potential field (due to the donor/acceptor frontier orbital energy offsets, e.g., δE as shown in Fig. 2) would then separate the exciton quickly into a radical ion pair with a free electron at acceptor LUMO and a free hole at donor HOMO, provided this field (or energy offset) is close

to an optimal value or range as discussed in section 4 of this paper. For a derivatized PPV donor and fullerene acceptor binary system, it was experimentally observed that the photo induced charge separation process at the PPV/fullerene interface was orders of magnitude faster then either the PPV exciton decay or the charge recombination [7, 8]. This means, opto-electronic quantum efficiency at the interface is near unity, and high efficiency organic photovoltaic system is feasible.

2.4. Carrier diffusion to the electrodes

Once the carriers (free electrons or holes) are generated, holes need to diffuse toward the positive large work function electrode (LWFE), and electrons need to diffuse toward the negative small work function electrode (SWFE). The driving forces for the carrier diffusion may include the field created by the work function difference between the two electrodes, as well as a 'chemical potential' driving force [24]. In an organic donor/acceptor binary photovoltaic cell, for instance, high-density electrons at the acceptor LUMO nearby the donor/acceptor interface tend to diffuse to lower electron density region within the acceptor phase, and high-density holes at the donor HOMO nearby the donor/acceptor interface tend to diffuse to the lower holes density region within the donor phase. For instance, in 'Tang Cell' as shown in Fig. 1b, at the D/A interface, once an exciton was separated into a free electron at acceptor side and a free hole at donor side, the electron will be 'pushed' away from the interface toward the negative electrode by both the 'chemical potential' and by the field formed from the two electrode work functions. The holes will be 'pushed' toward the positive electrode by the same forces but in the opposite direction. With this chemical potential force, even if the two electrodes are the same (i.e., the driving force due to work function difference does not present), asymmetric photovoltage could still be achieved (i.e., the donor HOMO would generate the positive electrode, and acceptor LUMO would form the negative electrode) [24]. Mid-gap state species, such as impurities and defects, or intentionally doped redox species, can also facilitate the charged carrier generation and diffusion by providing 'splitting' interfaces and 'hopping' orbitals. However, right after electron-hole is separated at the interface, it can also recombine due to both the potential drop between the acceptor LUMO and donor HOMO, and the Coulomb force between the electron and the hole. Fortunately, the charge recombination rates in most cases are much slower then the charge separation rates (e.g., charge recombination rates are typically in micro to milliseconds as compared to femto/pico seconds charge separation rate) [7, 8, 36], so there is an opportunity (in time domain) for the carriers to reach the electrodes before they recombine. In most currently reported organic solar cells, however, the diffusion of electrons and holes to their respective electrodes are not really smooth due to materials poor morphology. If donor and acceptor phases are perfectly 'bicontinuous' between the two electrodes, and all LUMO and HOMO orbitals are nicely aligned and overlapped to each other in both donor and acceptor phases, like in a molecularly self-assembled thin films or crystals, then the carriers should be able to diffuse smoothly in 'bands' toward their respective electrodes. Currently, carrier thermal 'hopping' and 'tunneling' are believed to be the dominant diffusion and conductivity mechanism for most reported organic photovoltaic systems, therefore, the "carrier loss" is believed to be another key factor for the low efficiency of organic photovoltaic materials and devices.

2.5. Carrier collection at the electrodes

It has been proposed [9] that when the acceptor LUMO level matches the Fermi level of the small work function electrode (SWFE), and the donor HOMO matches the Fermi level of the large work function electrode (LWFE), an ideal 'Ohmic' contact would be established for efficient carrier collection at the electrodes. So far, there are no organic photovoltaic cells have achieved this desired 'Ohmic' contacts due to the availability and limitations of materials and electrodes involved. There were a number of studies, however, focusing on the open circuit voltage (V_{oc}) dependence on materials LUMO/HOMO level changes, electrode Fermi levels, and chemical potential gradients [20, 24]. The carrier collection mechanisms at electrodes are relatively less studied and are not well understood. It is believed that the carrier collection loss at the electrodes is also a critical contributing factor for the low efficiency of existing organic solar cells.

3. Optimizations at spatial domains via a −DBAB- type block copolymer

3.1. Block copolymers and self-assembled supra-molecular nano structures

Block copolymer solid melts are known to exhibit behavior similar to conventional amphiphilic systems such as lipid-water mixtures, soap, and surfactant solutions [25, 26]. The covalent bond connection between distinct or different blocks imposes severe constraints on possible equilibrium states. This results in unique supra-molecular nano-domain structures such as lamellae (LAM), hexagonally (HEX) packed cylinders or columns, spheres packed on a body-centered cubic lattice (BCC), hexagonally perforated layers (HPL) and at least two bi-continuous phases: the ordered bicontinuous double diamond phase (OBDD) and the gyroid phase [25, 26]. The morphology of block copolymers is affected by chemical composition, block size, temperature, processing, and other factors. The block copolymer approach to photovoltaic functions offers some intrinsic advantages then the bilayer or composite/blend systems [13, 14, 27–35]. For instance, the phase separation between the two blocks of a MEH-PPV/polystyrene (with partial C_{60} derivatization on polystyrene block) donor/acceptor diblock copolymer system was indeed observed [13]. The polystyrene/C_{60} acceptor block is, however, not a conjugated chain system, the known poor electron mobility or "carrier loss" problem in polystyrene phase still remains an issue.

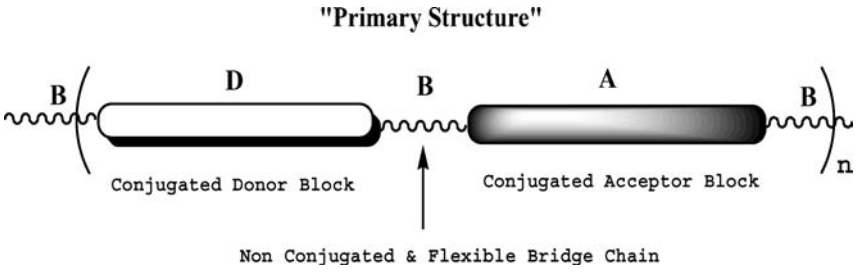

Figure 4 Scheme of a −DBAB- type of block copolymer "primary structure".

On the other hand, when a conjugated donor block was linked directly to a conjugated acceptor block to form a direct *p-n* type conjugated diblock copolymer, while energy transfer from higher gap block to lower gap block were observed, no charge separated states (which is critical for photovoltaic functions) were detected [27].

3.2. Design and development of a −DBAB- type block copolymer for a 'tertiary' supra-molecular nano structure

In order to address all the 'loss' problems of organic photovoltaic discussed above, particularly the 'exciton loss' and the 'carrier loss' problems which can be minimized in spatial domain optimizations, a photovoltaic device based on a −DBAB- type of block copolymer and its potential 'tertiary' supra-molecular nano structure was designed (Figs 4–9) [14]. In this design, *D* is a π electron conjugated donor block, *A* is a conjugated acceptor block, *B* is a non-conjugated and flexible bridge unit with its HOMO level lower then the acceptor HOMO, and its LUMO level higher then the donor LUMO, so that a potential barrier is formed between the donor and acceptor conjugated blocks on the polymer chain (Fig. 5). This potential barrier separates the orbitals of the donor and acceptor blocks and retards the electron-hole recombination as encountered in the case of directly linked *p-n* type diblock conjugated copolymer system [27]. At the same time, intra- or inter-molecular electron transfer or charge separation can still proceed effectively through σ bonds or

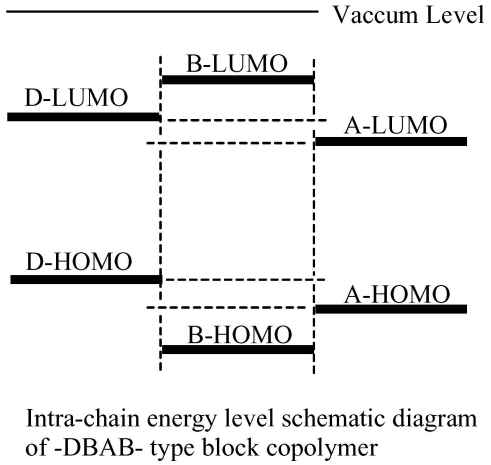

Figure 5 Scheme of a −DBAB- type of block copolymer relative energy levels.

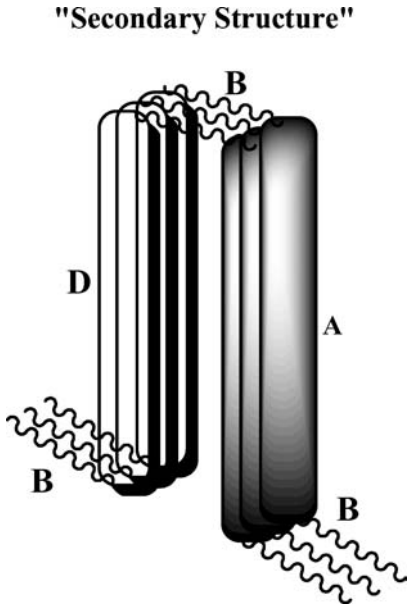

Figure 6 Scheme of a −DBAB- type of block copolymer "secondary structure".

through space under photo-excitations [36]. Additionally, the flexibility of the bridge unit would also enable the rigid donor and acceptor conjugated blocks to self-assemble and phase separate more easily, and be less susceptible to conjugation distortion. Since both donor and acceptor blocks are π electron conjugated chains, once they are self-assembled in a π-π stacking morphology as is well known in all π conjugated system [15] (Fig. 6), good carrier transport in both donor and acceptor phases now become feasible.

While the −DBAB- block copolymer backbone structure may be called "primary structure" (see Fig. 4), the conjugated chain π orbital closely stacked and ordered morphology may therefore be called "secondary structure" (Fig. 6). This "secondary structure" style has been known to dramatically enhance carrier mobility due to improved π orbital overlap as demonstrated in ordered discotic type liquid crystalline phases [10, 37], or in derivatized and self-assembled regio-regular polythiophenes [38] or template aligned poly-*p*-pheylenevinylenes [39]. Most importantly, this 'secondary structure' as shown in Fig. 6 is desirable for the exciton diffusion in horizontal direction and charge transport in vertical direction, as it has been demonstrated that the exciton diffusion was most effective along the direction perpendicular to the conjugated chain, and carrier mobility is best along the chain direction [39]. Finally, through the adjustment of block

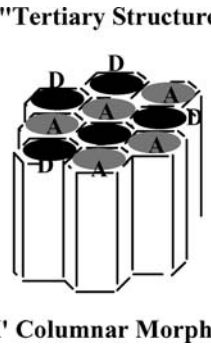

Figure 7 Scheme of a −DBAB- type of block copolymer "tertiary structure".

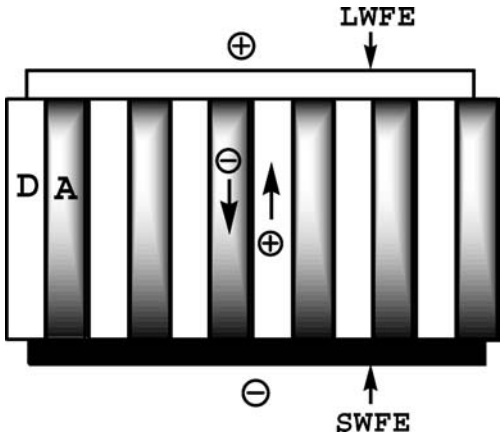

Figure 8 Scheme of a −DBAB- type of block copolymer solar cell in the form of columnar structure directly sandwiched between the two electrode layers.

size, block derivatization, and thin film processing protocols, a "tertiary structure" (Fig. 7) where a columnar or "HEX" type of morphology of the donor and acceptor blocks is vertically aligned on top of substrate and sandwiched between two electrodes is fabricated (Fig. 8). Even better, a thin donor layer may be inserted between ITO and active 'HEX' layer, and a thin acceptor layer is inserted between metal electrode and active 'HEX' layer to form an asymmetric D/A geometry. As a matter of fact, a diblock copolymer where a 'honey comb' type columnar structure was formed with either top or bottom of the 'honey comb' completely covered by one block has already been observed [40]. The terminal donor and acceptor layers would enable favorable chemical potential gradient for asymmetric (selective) carrier diffusion and collection at respective electrodes [6, 24]. Since the diameter of each donor or acceptor block column can be conveniently controlled via synthesis and processing to be within the organic average exciton diffusion length (AEDL) of 10–70 nm, so that every photo-induced exciton will be in convenient reach of a donor/acceptor interface along the direction perpendicular to the columnar. At the same time, photogenerated charge carriers can diffuse more smoothly to their respective electrodes via a truly "bicontinuous" block copolymer columnar morphology and long the conjugated chain direction. While the increased donor and acceptor interface area and phase morphology will dramatically minimize the exciton and carrier losses, it may nevertheless also increase the carrier recombination interfaces. However, by proper molecular frontier orbital level fine tuning, the charge recombination can be controlled to a much slower rate in comparison to the charge separation as discussed in Section 4 of this paper. For instance, in most reported organic photovoltaic systems, the charge recombination typically occurs on the microseconds or slower timescale, and this is in contrast to the ultra-fast pico- or femto- seconds charge separation rate at the same interface [8, 36]. Therefore, the charge carrier recombination does not appear to be of a major concern for solar cell applications where the radiation is continuous. Additionally, with appropriate adjustment of donor and acceptor block sizes and their substituents, energy levels, or with attachment of better photon energy matched sensitizing dyes on the polymer backbone, it is expected that the photon loss, the exciton loss, and the carrier loss (including charge recombination) issues can all be addressed and optimized simultaneously in one such block copolymer photovoltaic device. In order to examine the feasibility of this block copolymer solar cell design [14], a derivatized PPV −DBAB- type of block copolymer (Fig. 7) has already been synthesized and characterized, and some opto-electronic studies have already been in progress [28–35].

3.3. Materials, equipments, and experimental procedures

All starting materials, reagents and solvents were purchased from commercial sources and used directly except noted otherwise. Proton and carbon NMR data were obtained from a Bruker Avance 300 MHz spectrometer. Elemental analyses were done at Atlantic Microlab. HR-MASS and MALDI data were obtained from Mass Spectrometry facility at Emory University. Perkin-Elmer DSC-6/TGA-6 systems were used to characterize the thermal property of the materials. GPC analysis used a Viscotek T60A/LR40 Triple-Detector GPC system with mobile phase of THF at ambient temperature (Universal calibration based on polystyrene standards is used). UV-VIS spectra were collected from a Varian Gary-5 spectrophotometer. Luminescence spectra were obtained from an ISA Fluoromax-3 spectrofluorometer. Electrochemical analysis was done on a BAS Epsilon-100 unit. Film thicknesses were measured on a Dektek-6M profilometer. Thin film metal electrodes were deposited in high vacuum using a BOC-360 metal vapor deposition system. For dynamic spectroscopic studies, an Ar ion pumped and mode locked Ti-Sapphire laser system was used to create optical pulses at 800 nm and 120 femto seconds at 76 MHz.

Fig. 9 shows the chemical structures of the RO-PPV donor block (D), the SF-PPV-I acceptor block (A), the bridge units (B), and the general synthetic coupling scheme of the target −DBAB- block copolymer. Specifically, the donor block RO-PPV is an alkyloxy derivatized poly-*p*-phenylenevinylene, and the acceptor block SF-PPV-I is an alkyl-sulfone derivatized poly-*p*-phenylenevinylene. Two bridge units were used, first one is a long dialdehyde terminated bridge unit 1

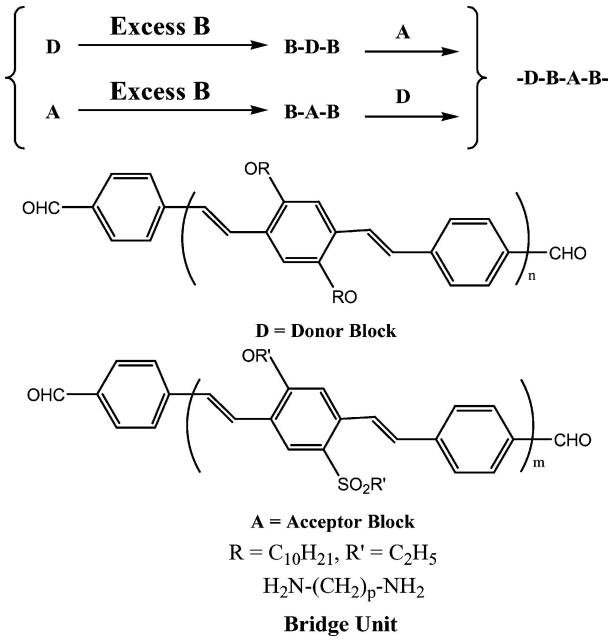

Figure 9 −DBAB- type conjugated block copolymer system already synthesized with a diamine bridge unit.

containing ten methylene aliphatic units, and the second one is a short diamine terminated bridge unit 2 containing two methylene units. When bridge unit 1 was used, both donor and acceptor blocks were synthesized with terminal phosphate groups. When diamine terminated bridge unit 2 was used, both donor and acceptor blocks were synthesized with terminal aldehyde groups. The alkyl derivatives (R) investigated includes branched 2-ethyl-hexyl group (C_8H_{17}), the ethyl (C_2H_5) and linear decacyl ($C_{10}H_{21}$) groups. The RO-PPV/SF-PPV-I based block copolymer syntheses have been reported elsewhere [28, 29, 34]. In this paper, only some key comparisons of the −DBAB- (with a two carbon diamine bridge unit 2) with a D/A blend system is presented. For biased dark current IV studies, the optoelectronic devices were fabricated by spin coating about 100 nm thick polymer films on top of ITO-glass substrates, and about 100 nm thick Al electrodes were thermally vacuum evaporated on top of polymer films. The active area between Al and ITO is about 1 × 2.5 cm^2. For photo current studies, the optoelectronic devices were fabricated by spin coating about 200 nm thick polymer films on top of half coated ITO-glass substrates, and about 100 nm thick Al electrodes were evaporated on top of polymer films. The light source was from an ISA Flurofax-3 luminescence spectrometer with 1 × 1 cm^2 beam size and about 0.01 Sun intensity. The active area between Al and ITO where the light will cover is about 1 × 1 cm^2.

3.4. Results and discussions on spatial domain optimizations

As elaborated earlier, the first critical step in organic photovoltaic is a photo-induced electron transfer from the donor to the acceptor (also called photo-doping) as shown in Figs 1–3, and this process can be characterized by a number of techniques, including photoluminescence (PL) quenching for radiative exciton decay, light-induced conductivity (photo current) measurements, light induced electron spin resonance (LIESR) spectroscopy, etc. [1–7]. Fig. 10 shows the solution absorption spectra of the RO-PPV donor block, the SF-PPV-I acceptor block, and the −DBAB- block copolymer. Since no obvious new bands were observed in the −DBAB- absorption spectrum in comparison to the spectra of D and A, therefore, there was no evidence of ground state 'chemical doping' in synthesized −DBAB-. Fig. 11 shows the solution PL emission spectra of the donor block, the acceptor block, and −DBAB- block in arbitrary units (because the PL emission from −DBAB- was too weak to be seen if on a same scale with D or A). From a molecular density-emission correlated analysis, it was found that the PL of −DBAB- was quenched by over 80% relative to the pristine donor or acceptor block in dilute solution [29]. This −DBAB- PL quenching was also confirmed by a much faster PL emission decay of −DBAB- (687 ps) versus the pristine donor or acceptor decay (1600 ps) [33]. Since the solutions were very dilute, the probability of inter-molecular photo induced charge separation or solid state defect trapping is very small, therefore, this over 80% PL quenching can be attributed mainly to intra-chain charge separation through the short bridge unit. This intra-chain electron transfer through a bridge energy barrier has been in fact widely observed before [36, 41, 42]. These results demonstrated that, a two carbon short bridge appears sufficient enough to separate the electronic structures of the RO-PPV donor and the SF-PPV-I acceptor blocks, yet it would still allow effective electron transfer through it. Fig. 12 shows the thin film absorption spectra of the RO-PPV donor block, the SF-PPV-I acceptor block, and −DBAB-. Again, no evidence of ground state electron transfer or 'chemical doping' was observed. Fig. 13 shows the thin film PL emission spectra of the donor block, the acceptor block, and the final −DBAB- block copolymer in arbitrary units. The PL emission of D/A blend films was similar to −DBAB-, yet with emission quenching varies from sample to sample, i.e., very sensitive to processing conditions. Again from a molecular density-emission correlated PL emission studies [29], it was

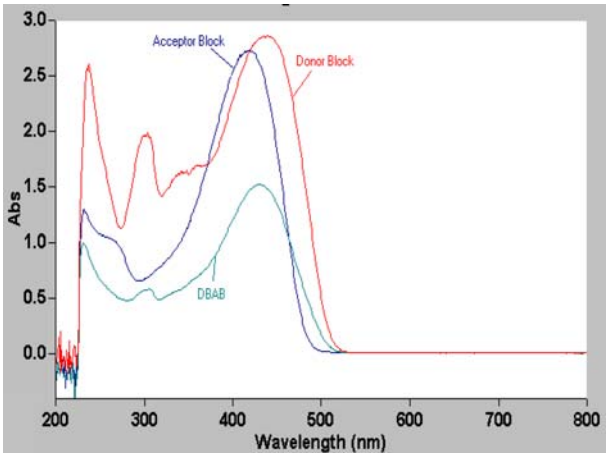

Figure 10 UV-VIS absorptions of RO-PPV (Donor), SF-PPV-I (Acceptor) and −DBAB- in dichloromethane.

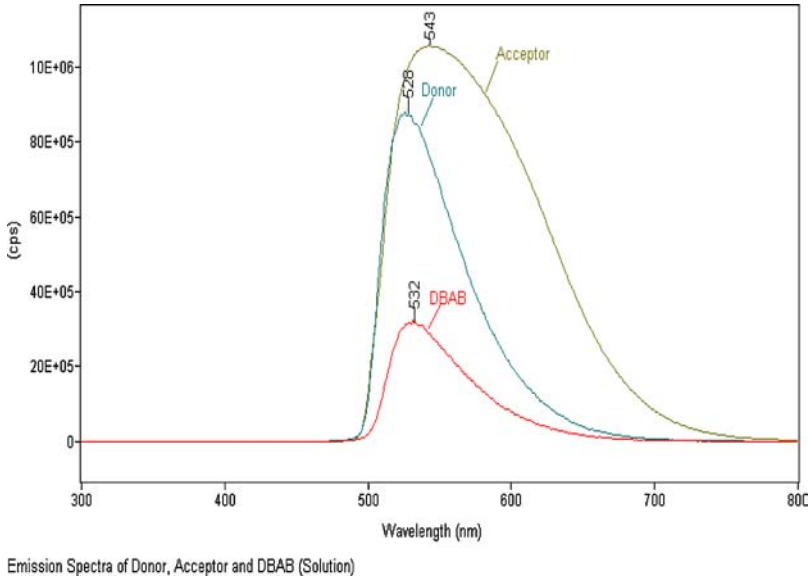

Figure 11 PL emissions of RO-PPV (D), SF-PPV-I (A), and −DBAB- in dichloromethane solution. The PL intensity (y-axis) is arbitrary for better view.

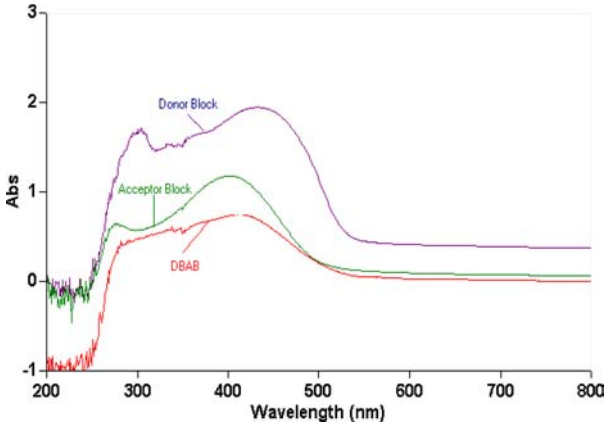

Figure 12 UV-VIS of RO-PPV (Donor), SF-PPV-I (Acceptor) and −DBAB- films on glass substrates.

found that the PL intensity of the blend films were typically quenched in the range of 10–70% relative to pristine donor or acceptor blocks, yet the PL emission of the final −DBAB- films were typically quenched at 90–99%. This strong PL quenching in −DBAB- film was also confirmed by a much faster PL emission decay of the −DBAB- films as compared to the D/A blend or pristine donor or acceptor films [33]. It is expected that this PL quenching enhancement of −DBAB- film was mainly due the photo induced inter-chain electron transfer from a donor block to a nearby acceptor block via close spatial contact. Clearly, such an inter-chain electron transfer enhancement is mainly due to the increase of the inter-molecular donor/acceptor interface and the improvement of the morphology of the −DBAB- block copolymer thin film. AFM and STEM studies revealed no any regular pattern in a D/A simple blend film under any conditions, yet some interesting regular pattern can be seen in −DBAB- block copolymer films at certain conditions [34]. Though details or mechanism of such pattern and its formation are unclear and are still under investigation, however, it is known that block copolymer morphology can be affected by many factors, such as chemical composition, block size, film substrates, processing conditions, etc. [25, 26]. For optoelectronic device comparison studies, as shown in Fig. 14, the dark voltage-current or IV data of a RO-PPV/SF-PPV-I (1:1 molar ratio blend film) was compared directly with a −DBAB- thin film, both films were spin coated in chloroform to about same thick device as elaborated in experimental part. Both thin film devices were thermally annealed at 140°C overnight. The Fig. 14 IV data shows that the biased dark current densities of −DBAB- were 2-3 orders higher then the D/A blend. For photo current studies, as Fig. 15 shows, the photo current density of −DBAB- was almost twice that of the D/A blend film at absorption peak (around 400 nm) under identical IV measurement conditions. Commercially available MEH-PPV/fullerene photo current was also measured under identical processing and measurement conditions, and as Fig. 15 shows, its photo current density was lower then the synthesized polymers. The dark current is also shown at the bottom of Figure 15. Both the open circuit voltage (V_{oc}) and short circuit current (I_{sc}) of these devices were very small, and it was due to several obvious and possible causes, such as primitive device fabrication (e.g., no any charge collection or injection buffer layers were used), PPV photo oxidative degradation in the air, etc. This is because very large photo currents were always observed at the initial moment when the light was irradiated to a freshly fabricated device in the air, and that PPV is well known for photo oxidative degradation [9]. The fact that the voltage biased dark current of −DBAB- were 2-3 orders of magnitude better then the D/A blend [35], and that photo current of −DBAB- was only doubled than the D/A blend may be explained as follows: in biased current, sufficient and same amount of charged carriers were injected from the electrodes for both −DBAB- films and D/A blend films. Therefore, the orders of magnitude current density differences can only be attributed to the main difference of the two films, i.e., the

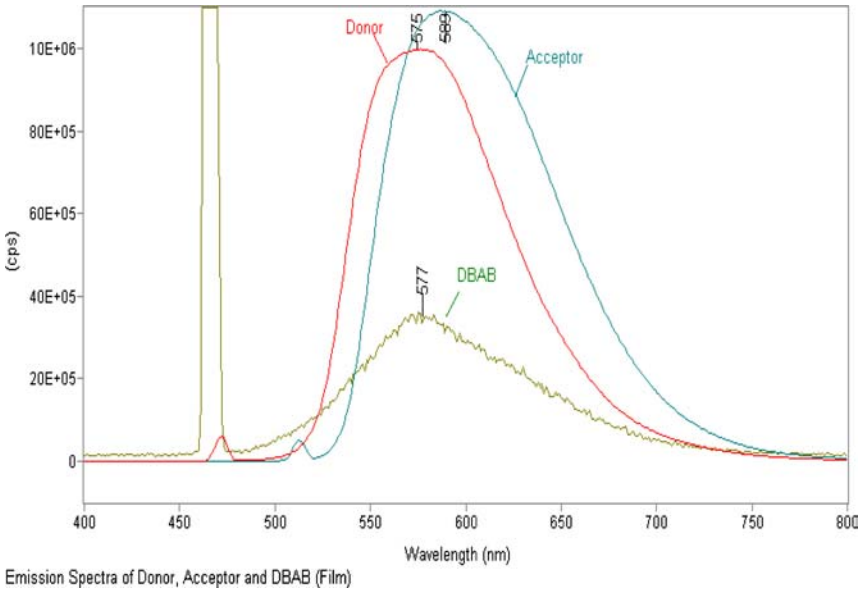

Figure 13 PL emissions of RO-PPV (D), SF-PPV-I (A), and −DBAB- thin films on glass substrates. The PL intensity (y-axis) is arbitrary for better view. (Note: the spikes at 470 and 510 nm are due to reflected excitation beam).

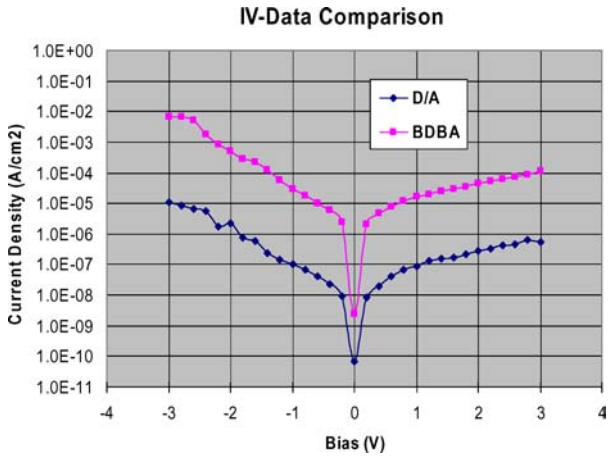

Figure 14 Voltage biased electric current density from thin films of −DBAB- block copolymer and D/A blend. Both films have the same materials density, same thickness and same electrode area.

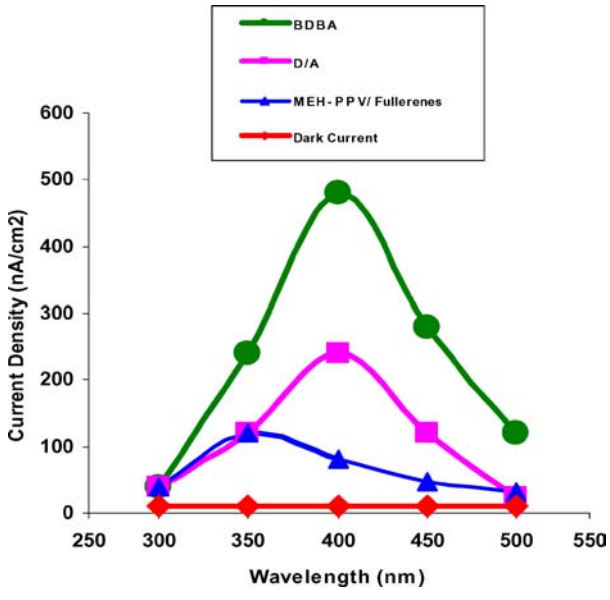

Figure 15 Photo current comparisons of several organic thin film photovoltaic cells.

much better spatial 'bicontinuous' transportation pathway or morphology in the −DBAB- film than in the D/A blend film. However, in photo current situations, even if the −DBAB- film has a much better spatial 'bicontinuous' transportation pathway then the D/A blend film, the photo generated carriers may be limited in both −DBAB- and D/A films due to either limited interface, improper energy levels, etc., therefore, the photo current difference was not as large as in biased situation. Optimizations of materials chemical structures, energy levels, morphological controls, device fabrication and measurements are ongoing and details will be reported separately.

4. Optimization in energy/time domain

4.1. Background

To address the optimal energy levels in a paired donor/acceptor organic light harvesting system, first, both the donor and acceptor optical excitation energy gaps should match the intended photon energy. For instance, in solar light harvesting applications, maximum solar photon flux is between 1.3–2.0 eV on the surface of the earth (AM = 1.5) and 1.8–3.0 eV in outer space (AM = 0) [1–3]. For optical telecommunications and signal processing, an optical excitation gap of 0.8 eV (for 1.55 micron IR signal) is needed. The excitation energy gaps in both the donor and the acceptor can be tuned via molecular design and engineering to match the photon energy, as both can absorb photon and incur charge separation at the donor/acceptor interface as shown in Figs 2–3. A critical remaining question is the magnitude of the frontier orbital energy level offset (δE as shown in Fig. 2) between the donor and the acceptor which is the key driving force for the charge separation. A current widely cited view is that δE should at least overcome the exciton binding energy (E_B), i.e., the minimum energy needed to overcome mainly the Coulomb electric forces to separate the intra-molecular

excitons into separate or 'free' inter-molecular electrons and holes [17]. Indeed when the energy offset of the donor/acceptor pair is too small, charge separation appears to become less efficient [41]. However, in many positive energy offset situations (such as in electron transfer from the donor to the acceptor via a higher energy level bridge unit as in many DBA systems), election transfer or charge separation still proceeds effectively [36, 42–45]. Albeit, if the energy offset is too large, Marcus 'inverted' region may result in a slow down of charge separation [42–45, 50], charge recombination may become severe, and thermal ground state charge separation without photo excitation may also occur. These are not desirable for light harvesting purposes. Large energy offset also reduces the open circuit voltage of the system [20]. Therefore, a systematic analysis of optimal donor/acceptor energy offsets is necessary in order to achieve efficient charge separation, particularly in consideration of exciton decay, charge separation and recombination processes in both the donor and the acceptor [46–48].

4.2. Formulation

In an ideal organic donor/acceptor type solar cell, both the donor and the acceptor should be able to harvest photons and contribute to the photovoltaic functions. The electron transfer processes may be simplified as follows (also illustrated in Figs 2–3):

(1) Photo excitation of the donor ($D/A + h\nu_1 \rightarrow D^*/A$, where D^* designates a donor exciton, $h\nu_1$ is the absorbed photon energy, and can be estimated from UV-VIS absorption or excitation spectra).

(2) Donor exciton decay to its ground state ($D^*/A \rightarrow D/A + h\nu_2$) corresponding to a standard Gibbs free energy change of E_D, decay rate constant of k_{dD}, and a reorganization energy of λ_{dD} [42–45]. $h\nu_2$ is the emitted photon energy, and can be estimated from photoluminescence (PL) emission spectra.

(3) Charge separation or electron transfer from the donor LUMO to the acceptor LUMO ($D^*/A \rightarrow D^+A^-$) corresponding to a free energy change of ΔE, electron transfer rate constant of k_{sD}, and a reorganization energy of λ_{sD}.

(4) Charge recombination or electron back transfer from the acceptor LUMO to the donor HOMO ($D^+A^- \rightarrow D/A$) corresponding to a free energy change of $E_r = E_D - \Delta E$, transfer rate constant of k_r, and a reorganization energy change of λ_r.

(5) Photo excitation at the acceptor ($D/A + h\nu_3 \rightarrow D/A^*$, where A^* designates an acceptor exciton).

(6) Acceptor exciton decay to its ground state ($D/A^* \rightarrow DA + h\nu_4$) corresponding to a free energy change of E_A, decay rate constant of k_{dA}, and a reorganization energy of λ_{dA}.

(7) Charge separation or electron transfer from the donor HOMO to the acceptor HOMO ($D/A^* \rightarrow D^+A^-$) corresponding to a free energy change of $E_{sA} = E_A - E_D + \Delta E$ (see Fig. 2), transfer rate constant of k_{sA}, and a reorganization energy of λ_{sA}.

(8) Charge recombination, the same process as described in 4).

For organic solar cell purpose, photo induced charge separated state (D^+A^-) is the desired starting point. However, first, charge separation (steps 3 or 7) is competing with exciton decay (steps 2 or 6). The ratio of the rate constants of charge separation versus exciton decay can therefore be defined as Exciton Quenching Parameter (EQP, mathematically represented as Y_{eq}), e.g., the donor exciton quenching parameter, Y_{eqD}, can be written as Equation 1 and the acceptor exciton quenching parameter, Y_{eqD}, can be written as Equation 2.

$$Y_{eqD} = k_{sD}/k_{dD} \tag{1}$$

$$Y_{eqA} = k_{sA}/k_{dA}. \tag{2}$$

Y_{eq} parameter reflects efficiency of exciton → charge conversion process. For instance, it was experimentally observed that the charge separation can be orders of magnitude faster then the exciton decay in a MEH-PPV/fullerene donor/acceptor binary pair [4]. Secondly, charge separation (steps 3 or 7) is also competing with charge recombination (steps 4 or 8). The ratio of charge separation rate constant over charge recombination rate constant may therefore be defined as Recombination Quenching Parameter (RQP, mathematically represented as Y_{rq}). The recombination quenching parameters for the donor and the acceptor are given by Equations 3 and 4 respectively.

$$Y_{rqD} = k_{sD}/k_r \tag{3}$$

$$Y_{rqA} = k_{sA}/k_r \tag{4}$$

For any light harvesting applications, including solar cell applications, it is desirable that both the Y_{eq} and Y_{rq} parameters are large.

From classic Marcus electron transfer theory [42–45], the electron transfer rate constants may be simplified as

$$k_{dD} = A_{dD} \exp[-(E_D + \lambda_{dD})^2/4\lambda_{dD}kT] \tag{5}$$

$$k_{sD} = A_{sD} \exp[-(\Delta E + \lambda_{sD})^2/4\lambda_{sD}kT] \tag{6}$$

$$k_r = A_r \exp[-(E_D - \Delta E + \lambda_r)^2/4\lambda_r kT] \tag{7}$$

$$k_{dA} = A_{dA} \exp[-(E_A + \lambda_{dA})^2/4\lambda_{dA}kT] \tag{8}$$

$$k_{sA} = A_{sA} \exp[-(E_A - E_D + \Delta E + \lambda_{sA})^2/4\lambda_{sA}kT] \tag{9}$$

$$A_y = \left(2\pi H_y^2/h\right)(\pi/\lambda_y kT)^{1/2} \tag{10}$$

Where $y = dD, sD, r, dA, sA$. H_y is an electronic coupling term between two electron transfer sites and can be estimated from molecular energy and dipole parameters using Mulliken-Hush model [42–45], λ_y is the reorganization energy containing contributions from molecular motions, vibrations, solvent effects, etc., and can be estimated from molecular vibrational spectroscopy or from excitation/emission spectroscopy under certain conditions [42–45]. T is temperature and

k is the Boltzman constant. The standard Gibbs free energy of E_D and E_A can be estimated from spectroscopic, electrochemical, and thermodynamic analysis [36, 42–45]. For instance, when ground and photo excited states free energy potential wells have similar shapes, the following apply [36]:

$$\lambda_{dD} = (h\nu_1 - h\nu_2)/2 \quad (11)$$

$$E_D = -(h\nu_1 + h\nu_2)/2 \quad (12)$$

$$\lambda_{dA} = (h\nu_3 - h\nu_4)/2 \quad (13)$$

$$E_A = -(h\nu_3 + h\nu_4)/2 \quad (14)$$

The charge separation free energy ΔE can be simplified as a charge separation driving force δE, and a charge separation counter-driving force E_B as:

$$\Delta E = \delta E + E_B \quad (15)$$

Where the driving force δE is the frontier orbital (LUMO-LUMO) energy offset between the donor and the acceptor (negative values), and E_B includes all counter-driving force terms, mainly electric Coulomb forces that need to be overcome in order to separate the inter-molecular exciton into a stable intra-molecular radical ion pair. E_B can be estimated from molecular/ionic parameters [36, 44, 45, 49]. In an organic solar cell, the electric fields nearby donor/acceptor interface due to electrode work functions are typically less then 0.001 V/nm, negligibly smaller then the typical exciton binding energy or the frontier orbital energy offset (on the order of 1 V/nm), and since the exciton binding energy is generally defined as the energy needed to separate an intra-molecular exciton (D^* or A^*) into an inter-molecular electron-hole radical ion pair (D^+A^-), E_B therefore can also be approximated as the exciton binding energy [13].

The donor Exciton Quenching Parameter EQP can thus be expressed as:

$$Y_{eqD} = k_{sD}/k_{dD} = (H_{sD}/H_{dD})^2(\lambda_{dD}/\lambda_{sD})^{1/2} \times \exp(Z_{eqD}) \quad (16)$$

where

$$Z_{eqD} = -(\delta E + E_B + \lambda_{sD})^2/4\lambda_{sD}kT + (E_D + \lambda_{dD})^2/4\lambda_{dD}kT \quad (17)$$

The acceptor Exciton Quenching Parameter EQP can thus be expressed as:

$$Y_{eqA} = k_{sA}/k_{dA} = (H_{sA}/H_{dA})^2(\lambda_{dA}/\lambda_{sA})^{1/2} \times \exp(Z_{eqA}) \quad (18)$$

where

$$Z_{eqA} = -(E_A - E_D + \delta E + E_B + \lambda_{sA})^2/4\lambda_{sD} \times kT + (E_A + \lambda_{dA})^2/4\lambda_{dA}kT \quad (19)$$

The donor Recombination Quenching Parameter RQP can be expressed as:

$$Y_{rqD} = k_{sD}/k_r = (H_{sD}/H_r)^2(\lambda_r/\lambda_{sD})^{1/2} \times \exp(Z_{rqD}) \quad (20)$$

where

$$Z_{rqD} = -(\delta E + E_B + \lambda_{sD})^2/4\lambda_{sD}kT + (E_D\delta E - E_B + \lambda_r)^2/4\lambda_r kT \quad (21)$$

And the acceptor Recombination Quenching Parameter RQP can be expressed as:

$$Y_{rqA} = k_{sA}/k_r = (H_{sA}/H_r)^2(\lambda_r/\lambda_{sA})^{1/2} \exp(Z_{rqA}) \quad (22)$$

where

$$Z_{rqA} = -(E_A - E_D + \delta E + E_B + \lambda_{sA})^2/4\lambda_{sA} \times kT + (E_D\delta E - E_B + \lambda_r)^2/4\lambda_r kT \quad (23)$$

4.3. Results and discussions

In this study, only the frontier orbital LUMO energy offset δE will be allowed to vary. For demonstration convenience, the following values are used: temperature $T = 300K$, $k = 0.000086$ eV/K, the calculated (from Equations 11–14) and estimated RO-PPV and SF-PPV-I data [28–35] of $E_D = -2.6$ eV, $E_A = -2.7$ eV, $E_B = -0.4$ eV, $\lambda_{sD} = \lambda_{sA} = 0.2$ eV, $\lambda_r = 0.5$ eV, $\lambda_{dD} = 0.4$ eV, $\lambda_{dA} = 0.6$ eV, and arbitrary data $H_x = 1 (x = sD, dD, sA, dA, r)$, a plot of normalized Y_{eqD}, Y_{eqA}, and $Y_{eq(D+A)} = Y_{eqD}Y_{eqA}$ versus δE is shown in Fig. 16.

As Fig. 16 illustrates, when the frontier LUMO orbital offset δE varies, Y_{eqD}, Y_{eqA}, and $Y_{eq(D+A)}$ all exhibit their own maximum values. Using $\partial Y_{eqD}/\partial\delta E = 0$, to determine the optimum exciton quenching value due to the donor excitation, gives Equation 24.

$$\delta E_{eqD} = -\lambda_{sD} - E_B = -0.6 \text{ eV} \quad (24)$$

This corresponds to a maximum donor exciton-charge conversion. Equation 24 implies when donor is excited, the optimum donor/acceptor LUMO-LUMO offset

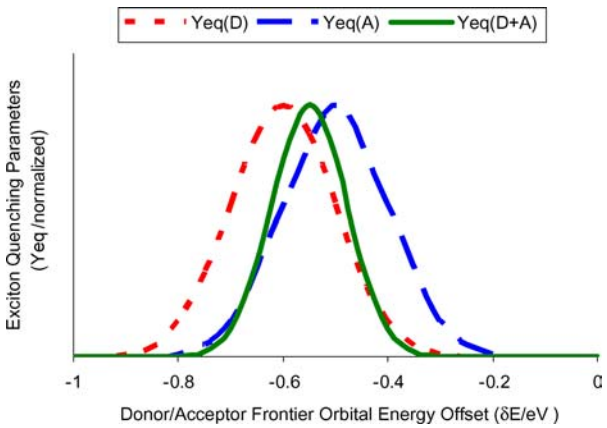

Figure 16 Exciton quenching parameters of the donor RO-PPV (left long dashed curve), acceptor SF-PPV-I (right short dashed curve), and their product $Y_{eq(D+A)} = Y_{eqD}Y_{eqA}$ (middle solid curve) versus the frontier LUMO orbital energy offset.

equals the sum of the donor charge separation reorganization energy and the exciton binding energy.

Using $\partial Y_{\mathrm{eqA}}/\partial\delta = 0$, to determine the optimum exciton quenching value due to acceptor excitation, gives Equation 25.

$$\delta E_{\mathrm{eqA}} = E_{\mathrm{D}} - E_{\mathrm{A}} - \lambda_{\mathrm{sA}} - E_{\mathrm{B}} = -0.5\ \mathrm{eV} \quad (25)$$

This corresponds to the most effective acceptor exciton-to-charge conversion. Equation 25 implies when the acceptor is excited, the optimum donor/acceptor HOMO-HOMO offset equals the sum of the acceptor charge separation reorganization energy and the exciton binding energy.

For the donor/acceptor pair where both can harvest light, the exciton quenching parameter for the pair can be expressed in Equation 26.

$$Y_{\mathrm{eq(D+A)}} = Y_{\mathrm{eqD}} Y_{\mathrm{eqA}} \quad (26)$$

Using $\partial Y_{\mathrm{eq(D+A)}}/\partial\delta E = 0$, to determine the optimum exciton quenching value of the pair, gives Equation 27.

$$\delta E_{\mathrm{eq(D+A)}} = [(E_{\mathrm{D}} - E_{\mathrm{A}})/\lambda_{\mathrm{sA}} - 2]/(1/\lambda_{\mathrm{sD}} + 1/\lambda_{\mathrm{sA}}) - E_{\mathrm{B}} = -0.55\ \mathrm{eV} \quad (27)$$

As can be seen from Fig. 16, $Y_{\mathrm{eq(D+A)}}$ represents an overlap area where both the donor and the acceptor can harvest photons simultaneously, and the optimum offset is around −0.55 eV. The actual RO-PPV/SF-PPV-I LUMO offset of −0.9 eV [29–35] appears a little larger then the optimum, thus RO-PPV/SF-PPV-I is in a so called 'Marcus inverted' region. Further improvement of photo induced charge separation can be realized via either reducing the RO-PPV LUMO level, or increasing the SF-PPV-I LUMO level.

For the donor recombination quenching parameter (RQP), from Equations 20–21, and using $\partial Y_{\mathrm{rqD}}/\partial\delta E = 0$, this gives Equation 28.

$$\delta E_{\mathrm{rqD}} = [2 + E_{\mathrm{D}}/\lambda_{\mathrm{r}}]/(1/\lambda_{\mathrm{r}} - 1/\lambda_{\mathrm{sD}}) - E_{\mathrm{B}} = 0.67\ \mathrm{eV} \quad (28)$$

This corresponds to a maximum $k_{\mathrm{sD}}/k_{\mathrm{r}}$ value.

For the acceptor recombination quenching parameter (RQP), from Equations 22–23, and using $\partial Y_{\mathrm{rq(A)}}/\partial g\delta E = 0$, this gives Equation 29.

$$\delta E_{\mathrm{rq(A)}} = [2 + (E_{\mathrm{A}} - E_{\mathrm{D}})/\lambda_{\mathrm{sA}} + E_{\mathrm{D}}/\lambda_{\mathrm{r}}]/(1/\lambda_{\mathrm{r}} - 1/\lambda_{\mathrm{sA}}) - E_{\mathrm{B}} = 0.83\ \mathrm{eV} \quad (29)$$

This corresponds to a largest $k_{\mathrm{s}}/k_{\mathrm{r}}$ ratio for SF-PPV-I acceptor.

For both the donor and the acceptor, the recombination quenching parameter can be expressed as:

$$Y_{\mathrm{rq(D+A)}} = k_{\mathrm{sA}} k_{\mathrm{sD}}/k_{\mathrm{r}} k_{\mathrm{r}} \quad (30)$$

Using $\partial Y_{\mathrm{rq(D+A)}}/\partial\delta E = 0$, this gives

$$\delta E_{\mathrm{rq(D+A)}} = [4 + (E_{\mathrm{A}} - E_{\mathrm{D}})/\lambda_{\mathrm{sA}} + 2E_{\mathrm{D}}/\lambda_{\mathrm{r}}]/(2/\lambda_{\mathrm{r}} - 1/\lambda_{\mathrm{sD}} - 1/\lambda_{\mathrm{sA}}) - E_{\mathrm{B}} = 0.75\ \mathrm{eV} \quad (31)$$

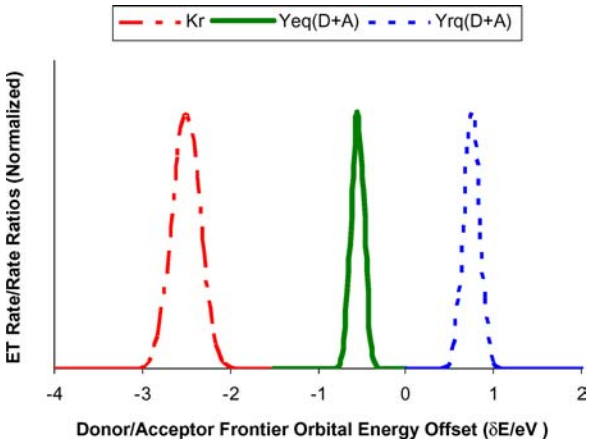

Figure 17 Exciton quenching parameter $Y_{\mathrm{eq(D+A)}} = k_{\mathrm{sD}}k_{\mathrm{sA}}/k_{\mathrm{dD}}k_{\mathrm{dA}}$ (middle solid curve), charge recombination rate constant k_{r} (left long dashed curve), and charge recombination quenching parameter $Y_{\mathrm{rq(D+A)}} = k_{\mathrm{sD}}k_{\mathrm{sA}}/k_{\mathrm{r}}k_{\mathrm{r}}$ (right short dashed curve) of the donor RO-PPV versus frontier LUMO orbital energy offset of the RO-PPV/SF-PPV-I pair when $\lambda_{\mathrm{r}} = 0.5$ eV.

The plots of $Y_{\mathrm{rq(D)}}, Y_{\mathrm{rq(A)}}$ and $Y_{\mathrm{rq(D+A)}}$ versus δE are similar to Fig. 16 except the X axis values are positive. Again, the $\delta E_{\mathrm{rq(D+A)}}$ value is between the donor and acceptor δE of highest Y_{rq}. Unfortunately, a positive δE value implies that the charge separation would be relatively slow, therefore, the Y_{rq} maximum appears to be insignificant in this case. It is desirable that $\delta E_{\mathrm{rq(D+A)}}$ is close to $\delta E_{\mathrm{eq(D+A)}}$.

To identify the most severe charge recombination, using $\partial k_{\mathrm{r}}/\partial\delta E = 0$ from Equation 7, this gives Equation 32.

$$\delta E_{\mathrm{r}} = E_{\mathrm{D}} + \lambda_{\mathrm{r}} - E_{\mathrm{B}} == -2.5\ \mathrm{eV} \quad (32)$$

The recombination rate constant k_{r}, the exciton quenching parameter $Y_{\mathrm{eq(D+A)}}$, and the charge recombination quenching parameter $Y_{\mathrm{rq(D+A)}}$ versus δE are plotted and shown in Fig. 17. As Fig. 17 shows, the optimum photo induced charge separation occurs at −0.55 eV which is the maximum overlap of the donor and acceptor Y_{eq}. For the donor (or the acceptor), as shown in Equations 24–25, the most efficient charge separation occurs where the LUMO (or HOMO) offset is equal to the sum of the exciton binding energy and the charge separation reorganization energy. The recombination become most severe at a LUMO offset of −2.5 eV, far away from optimum charge separation offset (−0.55 eV) as well as the actual RO-PPV/SF-PPV-I LUMO offset (−0.9 eV). Therefore, charge recombination in RO-PPV/SF-PPV-I pair does not seem to be of a major concern. An interesting note is that, during the charge separation, E_{B} represents the counter-driving Coulomb forces, while in charge recombination, E_{B} represents the driving Coulomb forces. Fig. 17 also shows that charge recombination quenching parameter $Y_{\mathrm{rq(D+A)}}$ does not reach its maximum until 0.67 eV, i.e., at a positive energy offset. At this positive energy offset, the photo induced charge separation might be too slow to be of attractive for efficient photovoltaic function. It is desirable that the $\delta E_{\mathrm{rq(D+A)}}$ is close to $\delta E_{\mathrm{eq(D+A)}}$, and that δE_{r} is far away from $\delta E_{\mathrm{eq(D+A)}}$.

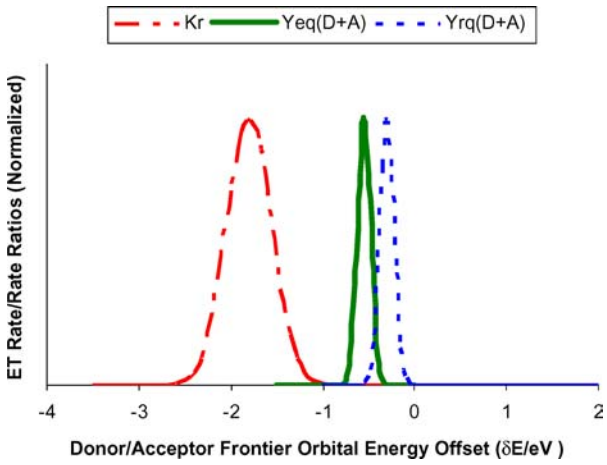

Figure 18 Exciton quenching parameter $Y_{eq(D+A)} = k_{sD}k_{sA}/k_{dD}k_{dA}$ (middle solid curve), charge recombination rate constant k_r (left long dashed curve), and charge recombination quenching parameter $Y_{rq(D+A)} = k_{sD}k_{sA}/k_rk_r$ (right short dashed curve) of the donor RO-PPV versus frontier LUMO orbital energy offset of the RO-PPV/SF-PPV-I pair when $\lambda_r = 1.2$ eV.

Assuming the molecules can be engineered such that the recombination reorganization energy $\lambda_r = 1.2$ eV, as Fig. 18 shows, the $\delta E_{rq(D+A)}$ would equal to -0.3 eV, very close to the $\delta E_{eq(D+A)}$ of -0.55 eV, yet $\delta E_r = -1.8$ eV, still far away from both optimum $\delta E_{eq(D+A)}$ and $\delta E_{rq(D+A)}$. However, if λ_r further increases to 2.2 eV, then as Fig. 19 shows, though $\delta E_{rq(D+A)}$ equals to -0.53 eV which is very close to the $\delta E_{eq(D+A)}$ of -0.55 eV, the δE_r would become -0.8 eV, also close to the optimum $\delta E_{eq(D+A)}$ of -0.55 eV. This means the charge separation would become a problem. It appears $\lambda_r = 1.2$ eV is an ideal situation to be considered for molecular design.

Like in any modeling/simulation studies, the numbers used here may not be accurate or important, rather, it is the trend that is the most important and meaningful. In order to further examine this model and prediction, a series and systematic experiments need to designed and performed. For Y_{eq} trend tests, when a donor (or acceptor) is fixed, as δE only changes charge separation rate constant k_s and not exciton decay rate constant k_d, it therefore can be regarded as a special case of 'Marcus inversion' case, and it has already been confirmed by experiments [42, 43, 50]. For Y_{rq} trend tests, since δE will change both k_s and k_r, therefore, a series donor/acceptor pairs where a donor (or an acceptor) is fixed first, and then a series acceptors (or a series of donors) with different δE in relation to the fixed donor (or acceptor) need to be experimentally evaluated for their charge separation and recombination rate constants. The type of experiments demonstrated in Ref. [50] are good examples, though no charge recombination rates and/or related reorganization energies were available at the same time to examine this model in detail. In future experiments, it is also important that the molecular structures of the changing acceptors (or donors) are similar, so that E_B and reorganization energies are similar, and that only the electronic withdrawing (or donating) strength (or δE) would be the major variable. In this way, δE versus the Y_{eq}, the Y_{rq} and the k_r can all be evaluated at the same time. The overall power conversion efficiency of the solar cell is expected to follow more closely Y_{eq} when both Y_{rq} and k_r are far away from Y_{eq}, and the cell efficiency can be evaluated at the same time, provided the charge transport and collection at electrodes are also similar. Unfortunately, these type of experiments have not yet been performed (or are not able to be performed) at the moment due to lack of suitable materials. Finally, additional parameters and competing processes (such as other electron and energy transfer processes) may also need to be taken into account in order to have a more accurate simulation. Systematic and expanded studies, including effects from molecular shapes, experimental case studies, etc., are underway and will be reported in the near future.

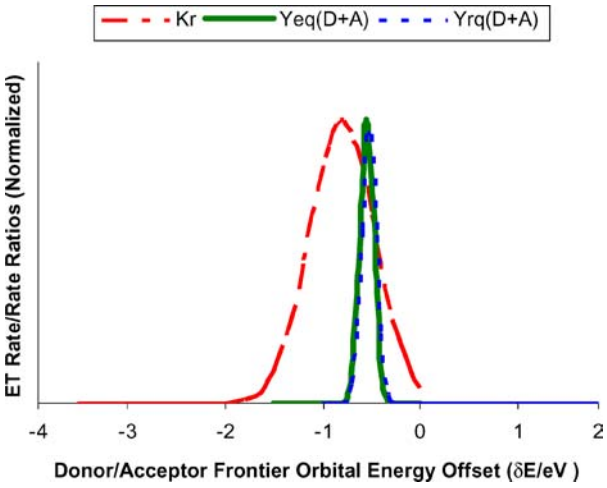

Figure 19 Exciton quenching parameter $Y_{eq(D+A)} = k_{sD}k_{sA}/k_{dD}k_{dA}$ (middle solid curve), charge recombination rate constant k_r (left long dashed curve), and charge recombination quenching parameter $Y_{rq(D+A)} = k_{sD}k_{sA}/k_rk_r$ (right short dashed curve) of the donor RO-PPV versus frontier LUMO orbital energy offset of the RO-PPV/SF-PPV-I pair when $\lambda_r = 2.2$ eV.

5. Conclusions

Current low photoelectric power conversion efficiencies of organic photovoltaic materials and devices can be attributed mainly to the 'photon loss', the 'exciton loss', and the 'carrier loss' due to improper frontier orbital energy levels/offsets and poor morphologies (or spatial geometries) for the charge carrier generation, transportation, and collection at electrodes. However, high efficiency organic photovoltaic materials and devices can be realized via optimizations in both space and energy/time domains.

In spatial domain optimizations, the key is a donor/acceptor nano phase separated and 'bicontinuous' morphology, where the dimension of each phase is within the average exciton diffusion length (i.e., 10–70 nm). For this reason, a −DBAB- type of block copolymer system and its potential 'tertiary' supramolecular columnar nano structure has been proposed and preliminary examined. In this system, along the carrier transport direction between the two electrodes, it is 'bicontinuous'. Yet on the direction parallel to the electrodes and perpendicular to the carrier transport direction, it is a nano phase separated periodic morphology, and each phase diameter is in the range of 10–70 nm.

The much improved PL quenching (from less then 70 to 99%), biased dark conductivity (2-3 orders of magnitude increase), and photo conductivity (100% increase) of the synthesized −DBAB- over the simple D/A blend system is attributed mainly to morphological (spatial) improvement, though such improvement has not yet been optimized.

In energy/time domain optimizations, first of all, the optical excitation energy gaps in both donor and acceptor are desired to match the photon energy, and that optimum donor/acceptor frontier orbital energy offsets corresponding to most efficient photo induced charge separation should be identified and materialized. Specifically, in electron transfer dynamic regime and based on classic Marcus electron transfer theory, this study has found that, there exists an optimal donor/acceptor energy offset where the exciton-to-charge conversion is most efficient (or exciton quenching parameter EQP reaches its maximum), and a second optimal energy offset where charge recombination is relatively slow compared to charge separation (or recombination quenching parameter RQP become largest). The molecules should be designed and developed such that the maximum RQP is close to or coincidence with maximum EQP. There also exists an undesired energy offset where charge recombination becomes most severe. The molecules should be designed and developed such that the energy offset corresponding to maximum charge recombination is far away from the energy offset where maximum EQP is located. For a donor/acceptor binary photovoltaic system, there also exists a fourth optimal donor/acceptor energy offset, where the EQP product of both donor and acceptor become largest, so that both donor and acceptor can effectively contribute to photo induced charge separation. Both the desired and undesired energy offsets are critically important for molecular structure and energy level fine tuning in developing high efficiency organic light harvesting systems, including organic photovoltaic cells, photo detectors, or any artificial photo-charge synthesizers/converters.

Acknowledgement

The authors are grateful for research/educational grant supports from a number of funding agencies including NASA, DOD (AFOSR, MDA), NSF, Department of Education, and Dozoretz foundation. Professor Sun is also very grateful to Professors C. Bonner, M. Wasielewski, J. Bredas, and in particular, R. Marcus for stimulating discussions on 'Marcus theory'.

References

1. M. D. ARCHER and R. HILL (eds.), "Clean Electricity From Photovoltaics" (Imperial College Press, London, 2001).
2. S. SUN and N. S. SARICIFTCI (eds.), "Organic Photovoltaics: Mechanisms, Materials and Devices" (CRC Press, Boca Raton, FL, 2005).
3. Z. KAFAFI and P. LANE (eds.), "Organic Photovoltaics IV" (SPIE, Bellingham, 2004).
4. C. BRABEC, V. DYAKONOV, J. PARISI and N. SARICIFTCI, "Organic Photovoltaics: Concepts and Realization" (Springer, Berlin, 2003).
5. A. HAGFELDT and M. GRAETZEL., *Acct. Chem. Res.* **33** (2000) 269.
6. C. TANG, *Appl. Phys. Lett.* **48** (1986) 183.
7. N. S. SARICIFTCI, L. SMILOWITZ, A. J. HEEGER and F. WUDL, *Science* **258** (1992) 1474.
8. B. KRAABEL, J. HUMMELEN, D. VACAR, D. MOSES, N. SARICIFTCI, A. HEEGER and F. WUDL, *J. Chem. Phys.* **104** (1996) 4267.
9. G. YU, J. GAO, J. HUMMELEN, F. WUDL and A. HEEGER, *Science* **270** (1995) 1789.
10. L. SCHMIDT-MENDE, A. FECHTENKÖTTER, K. MÜLLEN, E. MOONS, R. H. FRIEND and J. D. MACKENZIE, *Science* **293** (2001) 1119.
11. M. GRANSTROM, K. PETRITSCH, A. ARIAS, A. LUX, M. ANDERSSON and R. FRIEND, *Nature* **395** (1998) 257.
12. L. S. ROMAN, M. ANDERSON, T. YOHANNES and O. INGANAS, *Adv. Mater* **9** (1997)1164.
13. B. BOER, U. STALMACH, P. HUTTEN, C. MELZER, V. KRASNIKOV and G. HADZIIOANNOU, *Polymer* **42** (2001) 9097.
14. S. SUN, *Sol. Energy Mat. Sol. Cells* **79** (2003) 257.
15. T. A. SKOTHEIM, R. L. ELSENBAUMER and J. R. REYNOLDS, (eds.), "Handbook of Conducting Polymers," 2nd ed. (Marcel Dekker, New York, 1998).
16. J. PERLIN, "From Space to Earth-The story of Solar Electricity" (AATEC Publications, Ann Arbor, Michigan, 1999).
17. M. KNUPFER, *Appl. Phys. A* **77** (2003) 623.
18. T. STUBINGER and W. BRUTTING, *J. Appl. Phys.* **90** (2001) 3632.
19. H. AMERONGEN, L. VALKUNAS and R. GRONDELLE (eds.), "Photosynthetic Excitons" (World Scientific, Singapore, 2000).
20. C. BRABEC, *et al*., *Adv. Funct. Mater.* **11** (2001) 374.
21. C. BRABEC, C. WINDER, N. SARICIFTCI, J. HUMMELEN, A. DHANABALAN, P. HAL and R. JANSSEN, **12** (2002) 709.
22. N. SARICIFTCI, *et al*., *J. Poly. Sci., A.* **41** (2003) 1034.
23. V. SESHADRI and G. SOTZING, in "Organic Photovoltaics: Mechanisms, Materials and Devices," edited by, S. Sun and N. S. Sariciftci, (eds.), (CRC Press, Boca Raton, FL, 2005).
24. B. GREGG, *J. Phys. Chem. B.* **107** (2003) 4688.
25. N. HADJICHRISTIDIS, S. PISPAS and G. FLOUDAS (eds.), "Block Copolymers: Synthetic Strategies, Physical Properties, and Applications" (John Wiley & Sons, Inc., New York, 2003).
26. M. LAZZARI and M. LOPEZ-QUINTELA, *Adv. Mater.* **15** (2003) 1584.
27. X. L. CHEN and S. A. JENEKHE, *Macromolecules* **29** (1996) 6189.
28. S. SUN, Z. FAN, Y. WANG, C. TAFT, J. HALIBURTON and S. MAAREF, *SPIE Proc.* **4465** (2002) 121.
29. Z. FAN, "Synthesis and Characterization of A Novel Block Copolymer System Containing RO-PPV And SF-PPV-I Conjugated Blocks," MS Thesis, Norfolk State University, Norfolk, Virginia, July 2002.
30. S. SUN, Z. FAN, Y. WANG, J. HALIBURTON, C. TAFT, K. SEO and C. BONNER, *Syn. Met.* **137** (2003) 883.
31. S. SUN, Z. FAN, Y. WANG, C. TAFT, J. HALIBURTON and S. MAAREF, in "Organic Photovoltaics III," *SPIE* **4801** (2003) 114.
32. S. SUN, in "Organic Photovoltaics IV," SPIE, **5215** (2004) 195.
33. S. SUN and C. BONNER, "Chapter 8: Optimizations of Organic Solar Cells in Both Space and Energy/Time Domains," in *Organic Photovoltaics: Mechanisms, Materials and Devices*, edited by Sun and Sariciftci (CRC Press, Boca Raton, FL, 2005), pp. 183–214.
34. S. SUN, Z. FAN, Y. WANG, J. HALIBURTON, S. VICK, M. WANG, S. MAAREF, K. WINSTON, A. LEDBETTER and C. E. BONNER, "Development of a—Donor-Bridge-Acceptor-Bridge Type Block Copolymer for Potential Photovoltaic Applications," manuscript in preparation.
35. S. SUN, Z. FAN, Y. WANG, K. WINSTON and C. E. BONNER, *Mater. Sci. Eng. B.* **116** (2004) 279.
36. D. GOSZTOLA, B. WANG and M. R. WASIELEWSKI, *J. Photochem. Photobiol. (A)* **102** (1996) 71.

37. D. ADAM, P. SCHUHMACHER, J. SIMMERER, L. HAUSSLING, K. SIEMENSMEYER, K. ETZBACH, H. RINGSDORF and D. HAARER, *Nature* **371** (1994) 141.
38. Z. BAO, A. DODABALAPUR and A. J. LOVINGER, *Appl. Phys. Lett*. **69** (1996) 4108.
39. T. NGUYEN, J. WU, V. DOAN, B. SCHWARTZ and S. H. TOLBERT, *Science* **288** (2000) 652.
40. Private communication from Professor Marc Hillmyer.
41. S. SENSFUSS, *et al.*, "Characterization of Potential Donor Acceptor Pairs for Polymer Solar Cells by ESR, Optical and Electrochemical Investigations," in *Organic Photovoltaics IV*, edited by Z. Kafafi and P. Lane, *SPIE-proc.*, (2004) Vol. 5215, p. 129.
42. V. BALZANI (ed)., "Electron Transfer in Chemistry" (Wiley-VCH, New York, 2000).
43. R. MARCUS, *et al*., *J. Phys. Chem., B* **107** (2003) 6668.
44. E. PEETERS, P. HAL, J. KNOL, C. BRABEC, N. SARICIFTCI, J. HUMMELEN and R. JANSSEN, *ibid.* B **104** (2000) 10174.
45. J. BREDAS, *et al*., *J. Am. Chem. Soc.* **125** (2003) 8625.
46. S. SUN, "Organic Solar Cell Optimizations," project briefings to AFOSR and NASA, Spring, 2004.
47. *Idem*., "Sol. Energy Mater. Sol. Cells," **85** (2005) 261, published online on June 20, 2004.
48. *Idem*., *Mater. Sci. Eng*., *B*, **116** (2004) 251.
49. A. WELLER, *Z. Phys. Chem*. **133** (1982) 93.
50. J. MILLER, L. CALCATERRA and G. CLOSS, *J. Am. Chem. Soc*. **106** (1984) 3047.